ADVANCES IN ATMOSPHERIC SCIENCES, VOL. 39, APRIL 2022, 643–657

• **Original Paper** •

An Isentropic Mass Circulation View on the Extreme Cold Events in the 2020/21 Winter※

Yueyue YU*[1,2], Yafei LI*[3], Rongcai REN[2,1], Ming CAI[4], Zhaoyong GUAN[1], and Wei HUANG[5]

[1]*Key Laboratory of Meteorological Disaster, Ministry of Education (KLME)/Joint International Research Laboratory of Climate and Environment Change (ILCEC)/Collaborative Innovation Center on Forecast and Evaluation of Meteorological Disasters (CIC–FEMD) / Institute for Climate and Application Research (ICAR), Nanjing University of Information Science and Technology, Nanjing* 210044, *China*

[2]*State Key Laboratory of Numerical Modeling for Atmospheric Sciences and Geophysical Fluid Dynamics (LASG), Institute of Atmospheric Physics, Chinese Academy of Sciences, Beijing* 100029, *China*

[3]*Tianjin Meteorological Disaster Defense Technology Centre, Tianjin* 300074, *China*

[4]*Department of Earth, Ocean & Atmospheric Sciences, Florida State University, Tallahassee, Florida* 32304, *USA*

[5]*Key Laboratory of Mesoscale Severe Weather/Ministry of Education and School of Atmospheric Sciences, Nanjing University, Nanjing* 210044, *China*

(Received 26 July 2021; revised 2 November 2021; accepted 4 November 2021)

ABSTRACT

Three extreme cold events successively occurred across East Asia and North America in the 2020/21 winter. This study investigates the underlying mechanisms of these record-breaking persistent cold events from the isentropic mass circulation (IMC) perspective. Results show that the midlatitude cold surface temperature anomalies always co-occurred with the high-latitude warm anomalies, and this was closely related to the strengthening of the low-level equatorward cold air branch of the IMC, particularly along the climatological cold air routes over East Asia and North America. Specifically, the two cold surges over East Asia in early winter were results of intensification of cold air transport there, influenced by the Arctic sea ice loss in autumn. The weakened cold air transport over North America associated with warmer northeastern Pacific sea surface temperatures (SSTs) explained the concurrent anomalous warmth there. This enhanced a wavenumber-1 pattern and upward wave propagation, inducing a simultaneous and long-lasting stronger poleward warm air branch (WB) of the IMC in the stratosphere and hence a displacement-type Stratospheric Sudden Warming (SSW) event on 4 January. The WB-induced increase in the air mass transported into the polar stratosphere was followed by intensification of the equatorward cold branch, hence promoting the occurrence of two extreme cold events respectively over East Asia in the beginning of January and over North America in February. Results do not yield a robust direct linkage from La Niña to the SSW event, IMC changes, and cold events, though the extratropical warm SSTs are found to contribute to the February cold surge in North America.

Key words: isentropic mass circulation, extreme cold event, Stratospheric Sudden Warming, La Niña, Arctic sea ice, extratropical sea surface temperature

Citation: Yu, Y. Y., Y. F. Li, R. C. Ren, M. Cai, Z. Y. Guan, and W. Huang, 2022: An isentropic mass circulation view on the extreme cold events in 2020/21 Winter. *Adv. Atmos. Sci.*, **39**(4), 643−657, https://doi.org/10.1007/s00376-021-1289-2.

Article Highlights:

- The occurrence of cold extremes is closely related to a stronger equatorward cold air branch of the isentropic meridional mass circulation (IMC).
- Coupling between the poleward warm branch and the cold branch of the IMC via planetary waves accompanied the stratospheric sudden warming (SSW) event.
- The cold branch of the IMC strengthened over East Asia before the SSW event but strengthened over North America after the SSW event, causing the successive cold extremes.
- Low autumn sea ice and warm winter extratropical sea surface temperatures have a robust impact on the variability of the IMC in winter.

※ This paper is a contribution to the special issue on Extreme Cold Events from East Asia to North America in Winter 2020/21.

* Corresponding authors: Yueyue YU, Yafei LI
Email: yuyy@nuist.edu.cn, liyafei@lasg.iap.ac.cn

1. Introduction

Three extreme cold events invaded the midlatitude continents in the Northern Hemisphere in the 2020/21 winter. Two extreme cold events successively occurred over East Asia during 29–31 December 2020 and during 6–8 January 2021. The second extreme cold event is called the "boss level," with 58 meteorological stations in China observing the most extreme low temperatures since 1951 (Dai et al., 2021; Zhang et al., 2021). Furthermore, these two events were preceded by one moderately strong cold surge in the middle of December. Afterwards, another extreme cold event took place in North America during 5–22 February 2021, causing drastic and sudden temperature drops and setting new low-temperature records. Such extreme cold temperatures were combined with several rounds of snow and ice storms, leaving millions of people without power. Texas was hit particularly hard. A more detailed description of the three extreme cold events is given in Zhang et al. (2021). Such a frequent occurrence of extreme cold events within the same winter season is rarely seen, making the 2020/21 winter unique.

Another reason for the uniqueness of the 2020/21 winter is the remarkable anomalies of various forcing mechanisms on atmospheric general circulation, including tropical Pacific sea surface temperatures (SSTs), extratropical Pacific and Atlantic SSTs, and sea ice and the stratospheric polar vortex in the high latitudes (Fig. 1). These anomalies have been reported in many previous studies to be closely related to extreme cold events, and some pioneering studies have highlighted the 2020/21 winter (e.g., Dai et al., 2021; Zhang et al., 2021).

Firstly, observations show that La Niña conditions in the tropical Pacific developed, peaking in November 2020 as a moderate strength event (Fig. 1a) that persisted during February–April. Usually a La Niña event has a temporary global cooling effect. For East Asia, changes brought about by a La Niña event can lead to strengthened convection in the western Pacific, which favors cold air surges via the Pacific–East Asian teleconnection and an anomalous Walker circulation (Wang et al., 2000; Sakai and Kawamura, 2009; He and Wang, 2013; Abdillah et al., 2017; Ma and Chen, 2021). The weather impacts of La Niña events on North America are forced high pressure anomalies in the North Pacific and a northward shift of the winter storm track such that it passes through the Southwest United States less frequently. This leads to potentially fewer storms passing through the region. These circumstances increase the odds for above-/below- average precipitation and cold/warm temperatures in the Northeast/Southwest United States during cool-season months (e.g., Ropelewski and Halpert, 1986; Shabbar and Khandekar, 1996; Shabbar et al., 1997).

The extratropical ocean thermal anomaly in the 2020/21 winter was characterized by the significantly above-normal SSTs over the northeastern North Pacific and the northwestern Atlantic off the east coast of North America (Zhang et al., 2021), as shown in Figs. 1c–1d. The warm North Atlantic SSTs were in their strongest state around November–December 2020 and remained above-normal by more than one standard deviation until March 2021. The northeastern North Pacific was found to have even more abnormally warm SSTs (above normal by two to three standard deviations) until December, after which they gradually cooled back to normal. The 2020/21 winter extratropical SST anomalies over the North Pacific (Fig. 1e) resembled the negative phase of the North Pacific Gyre Oscillation (NPGO). Such warm SSTs over the northeastern North Pacific off the west coast of North America, as a local boundary forcing mechanism, have been demonstrated to be able to cancel out the cooling effect of La Niña over North America, leading to abnormal warmth there (Hoerling and Kumar, 1997; Shabbar and Yu, 2009). But such a relation is not always true. Taking the 2013/14 winter for instance, there was an NPGO-type marine heatwave event (Joh and Di Lorenzo, 2017), but there were extremely cold conditions in North America from January until early spring.

Meanwhile, the Arctic sea ice extent reached its second-lowest record since 1979 in September 2020 (NASA, 2020), and its anomaly fell below –2 standard deviations in October, as shown in Fig. 1b. Low sea ice extent in autumn modulates the meridional temperature gradient, which can effectively change the zonal wind, planetary waves, and midlatitude weather and climate in winter (Petoukhov and Semenov, 2010; Francis and Vavrus, 2012; Liu et al., 2012; Screen and Simmonds, 2013; Luo et al., 2016; Sorokina et al., 2016; Sun et al., 2016; Yao et al., 2017; Zhang et al., 2020).

Moreover, a Stratospheric Sudden Warming (SSW) event, which is the most dramatic stratospheric phenomenon, occurred in the beginning of January (Lee, 2021; Lu et al., 2021). This was a displacement-type SSW event based on the definition of Charlton and Polvani (2007), but it looked like a displacement-split type SSW event based on Choi et al. (2019, 2021) with an abnormally long duration (> 2 weeks). Accompanying this SSW event was the Arctic Oscillation in its negative phase at the surface, which lasted for two months. It is widely accepted that after an SSW event, the stratospheric circulation anomalies tend to propagate downward via wave-mean flow interaction, enhancing the negative phase of the Arctic Oscillation (AO) and cold events in the midlatitudes (Thompson et al., 2002; Kenyon and Hegerl, 2008; Tomassini et al., 2012; Huang and Tian, 2019). Particularly for vortex displacement events, cold anomalies tend to occur over the southeastern United States within one to two months after the central dates of SSW events, but they tend to occur over Eurasia during the one month ahead of the central dates of SSW events (Mitchell et al., 2013, Kidston et al., 2015; Lehtonen and Karpechko, 2016; Yu et al., 2018a). Choi et al. (2021) found that a displacement-split type SSW event always has the most robust response from the central to eastern North America cold events.

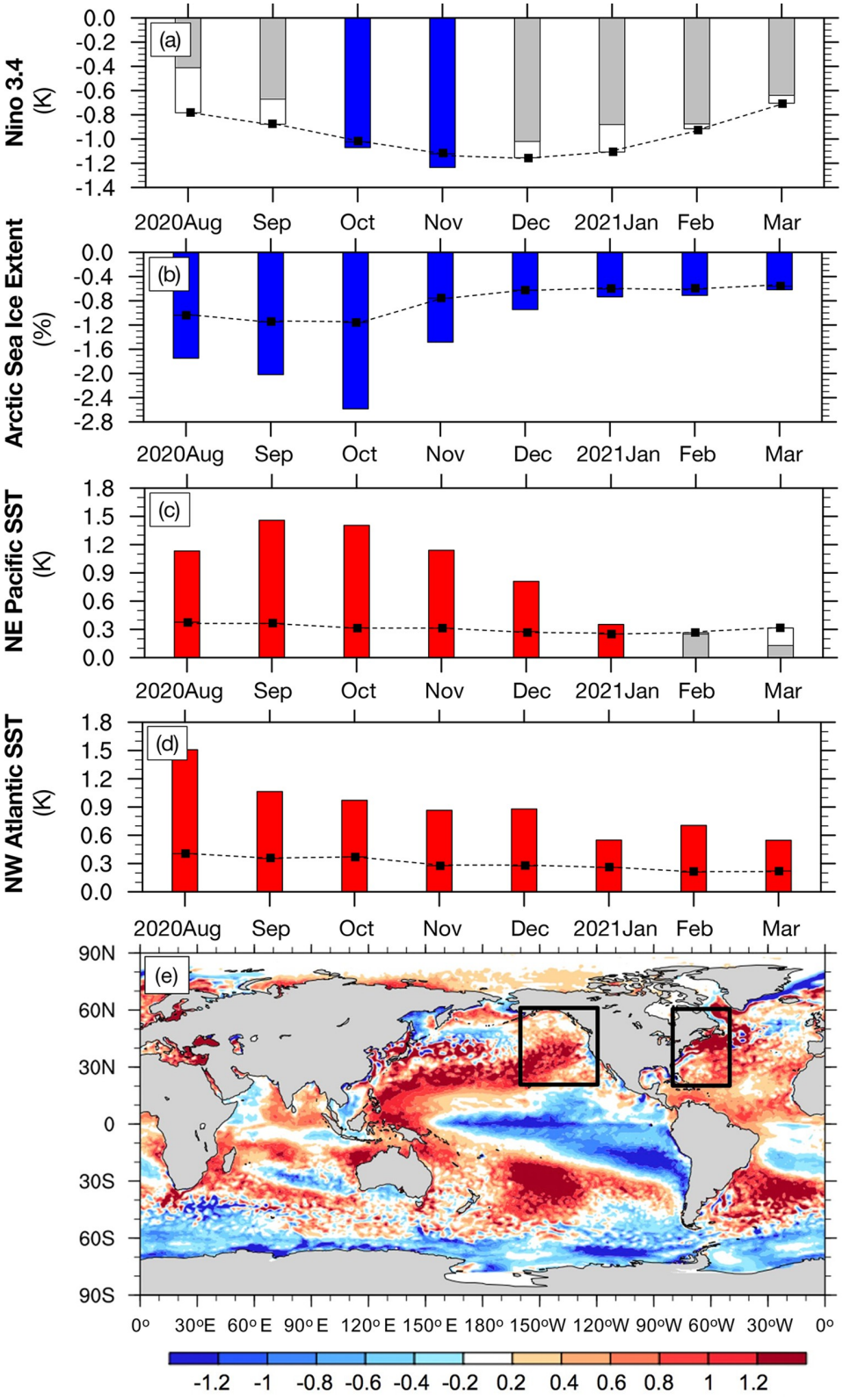

Fig. 1. Monthly time series of anomalies of (a) Niño-3.4 index, (b) Arctic sea ice extent index, (c) SST averaged over the northeastern Pacific region (120°–160°W, 20°–60°N), and (d) SST averaged over the northwestern Atlantic region (50°–80°W, 20°–60°N) from August 2020 to March 2021. (e) The 2020/21 winter (November–March) mean SST anomalies (units: K). The black boxes indicate the northeastern Pacific region and northwestern Atlantic region. Dots and dashed curves indicate the ±1 standard deviation for each month. Anomaly values below –1 standard deviation are highlighted by red or blue colored bars.

The isentropic meridional mass circulation (IMC) is essentially a Hadley-type mass circulation from the equator to the poles, forced by both diabatic heating/cooling and an eddy-induced forcing mechanism (Gallimore and Johnson, 1981; Townsend and Johnson, 1985; Johnson, 1989). With potential temperature as the vertical coordinate, the IMC framework naturally separates the warm and cold air masses and can be considered as a semi-Lagrangian view on the general circulation of the atmosphere. The IMC is comprised of net poleward mass transport in the upper isentropic layers (the warm air branch, denoted as WB) and an equatorward mass transport in the lower isentropic layers (the cold air branch, denoted as CB), as shown in Fig. 2a. In the extratropics, there is poleward mass transport leeward (east) of a trough and equatorward mass transport windward (west) of a trough (Fig. 2b). The climatological routes for the cold air intrusion are mainly through East Asia and North America (Fig. 2d), while the routes for warm air into the polar region are through the Pacific and Atlantic oceans (Fig. 2c). The driving force of the IMC in the midlatitudes and subpolar region is the presence of baroclinically amplifying waves, which lead to more warm air being transported poleward before a trough than being transported equatorward after a trough in the upper isentropic layers and more cold air being transported equatorward in the lower isentropic layers. In particular, the planetary waves, which are critical for stratosphere–troposphere coupling, play the dominant role in driving the hemispheric IMC and determining its variability (Yu et al., 2018c). Therefore, the IMC framework is perhaps the most direct way of viewing the cold air outbreaks and studying the linkage of cold air outbreaks to stratospheric variability (Iwasaki and Mochizuki, 2012; Iwasaki et al., 2014; Shoji et al., 2014; Yu et al., 2015a, b, c; Cai et al., 2016; Abdillah et al., 2017).

In this study, we intend to examine the characteristics of the IMC and associated cold and warm air activities to establish a physical linkage among the warm and cold air branches of the IMC, SSW, and extreme cold events that

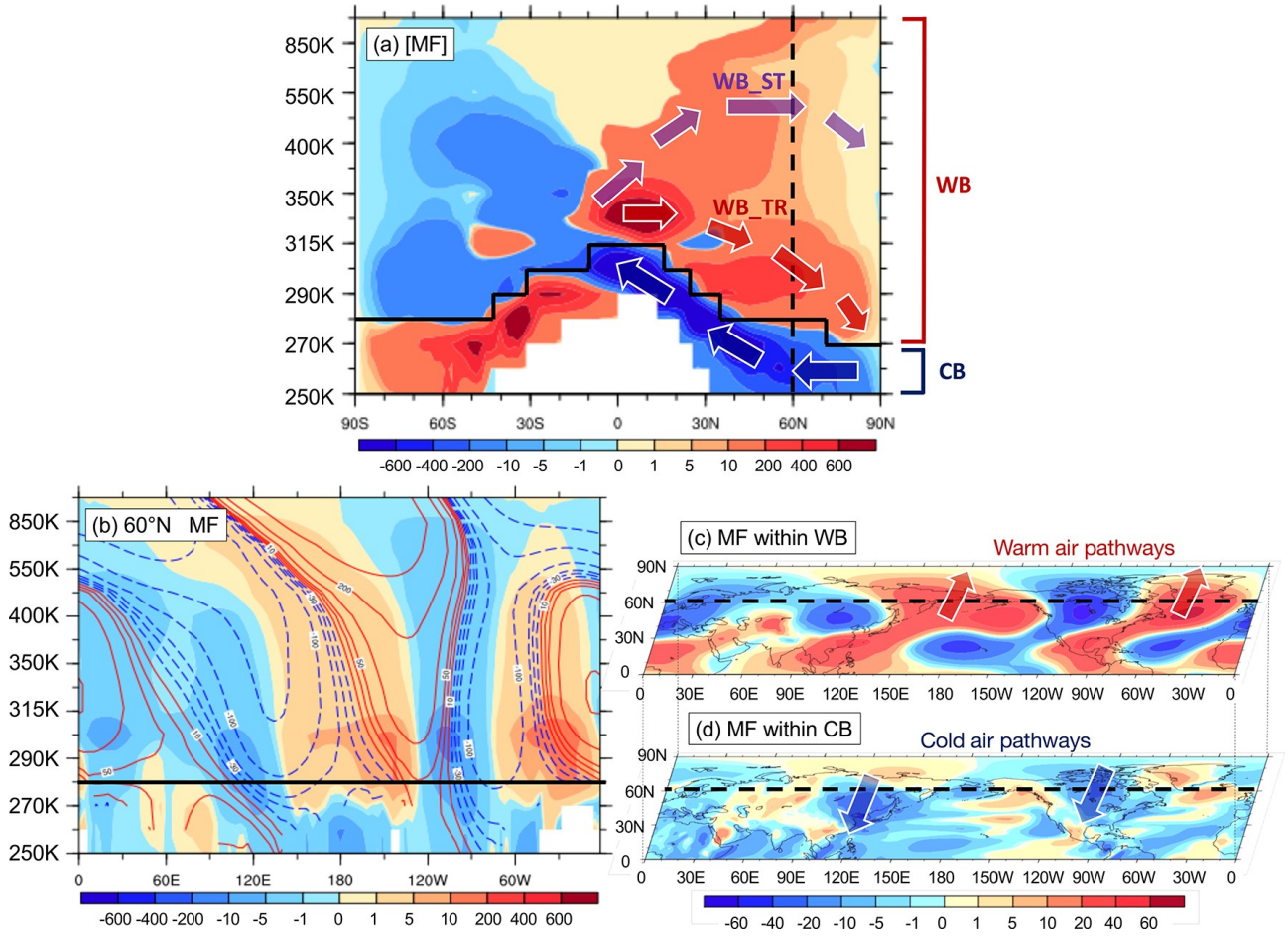

Fig. 2. Winter climatology of the isentropic meridional mass circulation (10^8 kg s^{-1}) derived from ERA-5 in the period 1980–2010. (a) Zonally integrated meridional mass flux at various latitudinal bands and isentropic layers, (b) meridional mass flux (shadings) and zonal deviation of geopotential height (contours) at 60°N at various isentropic layers, and the meridional mass flux vertically integrated within (c) the poleward warm branch (WB) and (d) the equatorward cold branch (CB) of the IMC. The black curve in panels (a) and (b) indicates the winter mean boundary isentropic level between the CB and WB. The dashed black line indicates 60°N. Arrows in panels (a, c, d) highlight the movement of air mass.

occurred in the 2020/21 winter. Through the following discussion on the relation of the IMC variability in winter with the tropical and extratropical SSTs and Arctic sea ice, this study helps advance our understanding of how background forcing contributes to the occurrence of record-breaking extreme cold events in the 2020/21 winter.

2. Data and methods

The datasets used in this study include the temperature (T2m), pressure (Ps), and meridional wind (v_s) at the surface and the three-dimensional air temperature (T), geopotential height (z), and meridional wind (v), which are derived from the 6-hourly ERA5 dataset [Copernicus Climate Change Service (C3S)] for the 42 winters from 1 November 1979 to 28 February 2021 (Hersbach et al., 2020). These data have a horizontal resolution of 1.5° × 1.5° and include 37 pressure levels from 1000 hPa to 1 hPa. Three-dimensional and surface potential temperature fields are obtained from the temperature fields at the various pressure levels.

We use the same methods as Yu et al. (2015a, b, c) to calculate variables associated with the IMC (including isentropic air mass and meridional mass fluxes as a function of potential temperature, longitude, and latitude) from daily fields. Each of the 42 winters lasts for 120 days from 1 November of the current year to 28 February of the next year.

We also analyze Plumb wave-activity fluxes to study the three-dimensional propagation of planetary waves, which are the main drivers of the IMC in the extratropics. By strictly following Plumb (1985), we derive the Plumb wave-activity flux from the geopotential, air temperature, and the zonal and meridional components of the geostrophic wind velocity. Since the magnitudes of wave-activity fluxes vary remarkably from the troposphere to the stratosphere, we multiply the fluxes by $\sqrt{1000/p}$ when plotting, in order to better present the propagating feature of Rossby waves.

The daily climatological-mean IMC and wave flux fields are obtained by averaging the data across the 42 years for each calendar day from 1 November to 28 February. Daily anomalies are obtained by removing the daily climatology from the total fields.

To measure the anomalous signals in the SST forcing, the Niño-3.4 index (https://psl.noaa.gov/data/timeseries/monthly/NINO34/) is used to denote the phase of ENSO. To be comparable to the 2020/21 winter, seven moderate and strong La Niña winters from 1979 to 2020 are selected (these events are defined by five consecutive overlapping three-month periods with Niño-3.4 anomalies at or below –1 K). The daily SST fields on a 0.25° × 0.25° grid are obtained from the NOAA High-resolution Blended Analysis of Daily SST (https://psl.noaa.gov/data/gridded/data.noaa.oisst.v2.highres.html). The northeastern Pacific mean SST is derived as the average over the box region of 120°–160°W, 20°–60°N, and the northeastern Atlantic mean SST is derived as the average over 50°–80°W, 20°–60°N. Abnormally warm extratropical SST years are selected when the monthly regional mean SST exceeds the climatological mean by at least one standard deviation.

Arctic sea ice change is measured by the satellite-retrieved sea ice extent (SIE) monthly data obtained from NSIDC (http://nsidc.org/data/seaice/data_summaries.html), and the low SIE years are defined when the September SIE is below normal by at least one standard deviation.

The information on historical displacement-type SSW events following the definition of Charlton and Polvani (2007) is obtained from Lehtonen and Karpechko (2016) for 1979–2016 and Rao et al. (2018, 2019), Lee (2021), and Lu et al. (2021) for 2017–21, respectively. Fifteen displacement-type SSW events in total were selected from the 42 winters (December–February) from 1979 to 2021.

3. Relationship among the IMC, SSW, and extreme cold events in the 2020/21 winter

3.1. *Physical linkage between the CB and cold events*

Displayed in Figs. 3c, 3f, and 3i are the anomaly fields of surface air temperature zonally averaged over entire latitude circles, East Asia (60°–145°E), and North America (90°–150°W), respectively. We can see two cold periods over midlatitude East Asia (i.e., 10–20 December and 25 December–10 January) and one cold period over midlatitude North America (i.e., 10–20 February). The cold temperatures in the midlatitudes were a direct result of the enhanced southward intrusion of the polar cold air mass, as manifested by the equatorward propagation of positive anomalies of isentropic air mass below 270 K (shadings in Figs. 3f and 3i). Accompanying the negative temperature anomalies and positive cold air mass anomalies in the midlatitudes were the positive temperature anomalies and negative cold air mass anomalies in the high latitudes. The cold air mass and surface temperature anomalies in high and middle latitudes exhibited almost out-of-phase variations over both East Asia and North America.

Seen from the evolution of meridional mass flux anomalies within the CB below 270 K respectively over the East Asian and North American sectors (bottom panels of Figs. 3e and 3h), there were negative meridional mass flux anomalies across the polar circle, indicating a strengthened equatorward transport of polar cold air over East Asia and North America several days before the cold/warm surface temperature anomalies in middle/high latitudes. Such leading relationships of the cold air transport of the IMC with extratropical temperatures can be seen more clearly from Figs. 4b and 4c. The strengthened equatorward cold air transport in East Asia and North America dominated the three rounds of strengthened CBs of the IMC and thus the cold air mass redistribution between the high and middle latitudes over entire latitudinal bands (bottom panel of Figs. 3b and 3c).

It is important to point out that the maximum intensities of the negative daily meridional mass flux over East

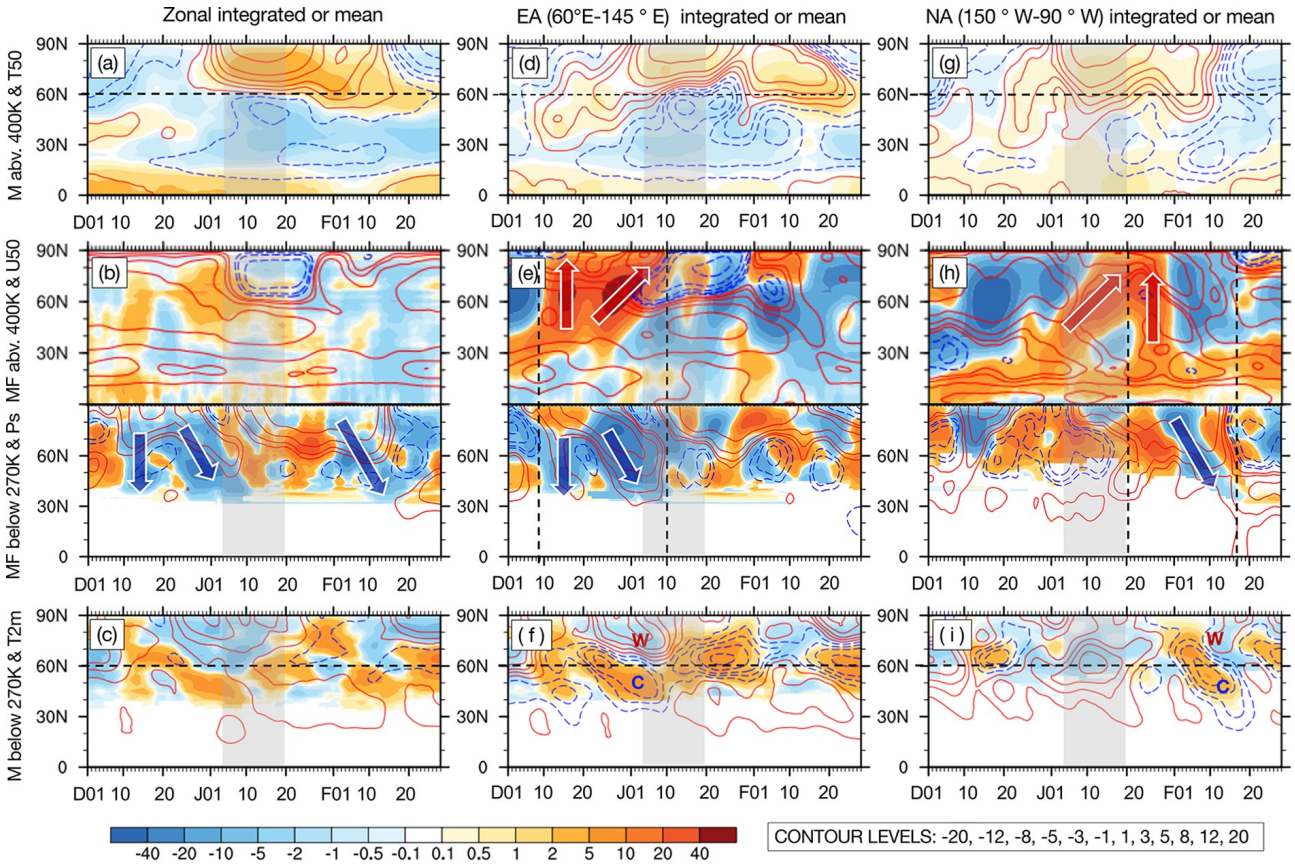

Fig. 3. The latitude-time evolution of anomaly fields of temperature, geopotential height, and the IMC and total field of zonal wind in the 2020/21 winter. (a) Zonally integrated air mass above 400 K (shadings, 10^{14} kg) and zonal mean temperature at 50 hPa (contours, K); (b) Zonally integrated meridional mass fluxes within the stratospheric component of warm branch of IMC (WB_ST) above 400 K and within the CB below 270 K (shadings, 10^9 kg s^{-1}), overlayed by zonal wind at 50 hPa (m s^{-1}) and surface pressure anomaly (hPa), respectively (contours); (c) Zonally integrated air mass below 270 K and zonal mean temperature near surface. (d–f) and (g–i) are the same as (a–c) but for zonal integration or zonal mean over the East Asian longitudinal range (60°–145°E) and North American longitudinal range (150°–90°W), respectively. The green box indicates the period of the SSW. Red and blue arrows highlight the poleward warm air transport and the equatorward cold air transport across 60°N.

Asia (25 December–10 January) and North America (10–20 February) exceed the 97th percentile of the historical records from 1979 to 2021. Such extremely strong equatorward cold air transport at 60°N in the 2020/21 winter brought an extra hundred billion tons of polar cold air mass into the midlatitude continental areas, explaining the record-breaking intensity of these extreme cold events.

3.2. *The coupling between the CB and WB responsible for the occurrence of the SSW event*

Next, we explain the relationship between the SSW and extreme cold events in the 2020/21 winter in view of the coupling between the equatorward CB and the stratospheric portion of the poleward WB of the IMC. Seen from the upper panels of Figs. 3e and 4a, over the East Asian sector, accompanied by the strengthened equatorward cold air transport, was a stronger poleward warm air mass transport in the stratosphere above 400 K in a quite long period from 9 December to 10 January. Such vertical coupling of meridional mass transport across the polar circle in opposite directions is expected to be achieved by stronger planetary waves of deep structure (Johnson, 1989; Yu and Ren, 2019). The regionally strengthened warm air mass adiabatically transported into the polar stratosphere dominantly contributes to the strengthened WB of the IMC across the entire latitude circle (upper panels of Figs. 3b and 4b), leading to a continuous increase/decrease in the total warm air mass within the polar/midlatitude stratosphere from December to mid-January (Fig. 3a). As a result, there were large positive anomalies of temperature at 50 hPa and total column mass above 400 K (proportional to pressure) in the polar region from the end of 2020 to mid-February 2021 (Figs. 3a, 3d, and 3g). Therefore, the accumulative effects of anomalous adiabatic mass transport due to dynamical processes lead to a significantly weakened stratospheric polar vortex at a lag time of about two weeks, consistent with Yu et al. (2018b).

Because the stronger poleward warm air mass transport is mainly over the East Asian sector with a maximum around 60°N, there was a loss of air mass in the middle latitudes but a gain of polar warm air mass in the East Asian sector. This explains the following negative anomalies of temperature at 50 hPa and mass above 400 K (proportional to pres-

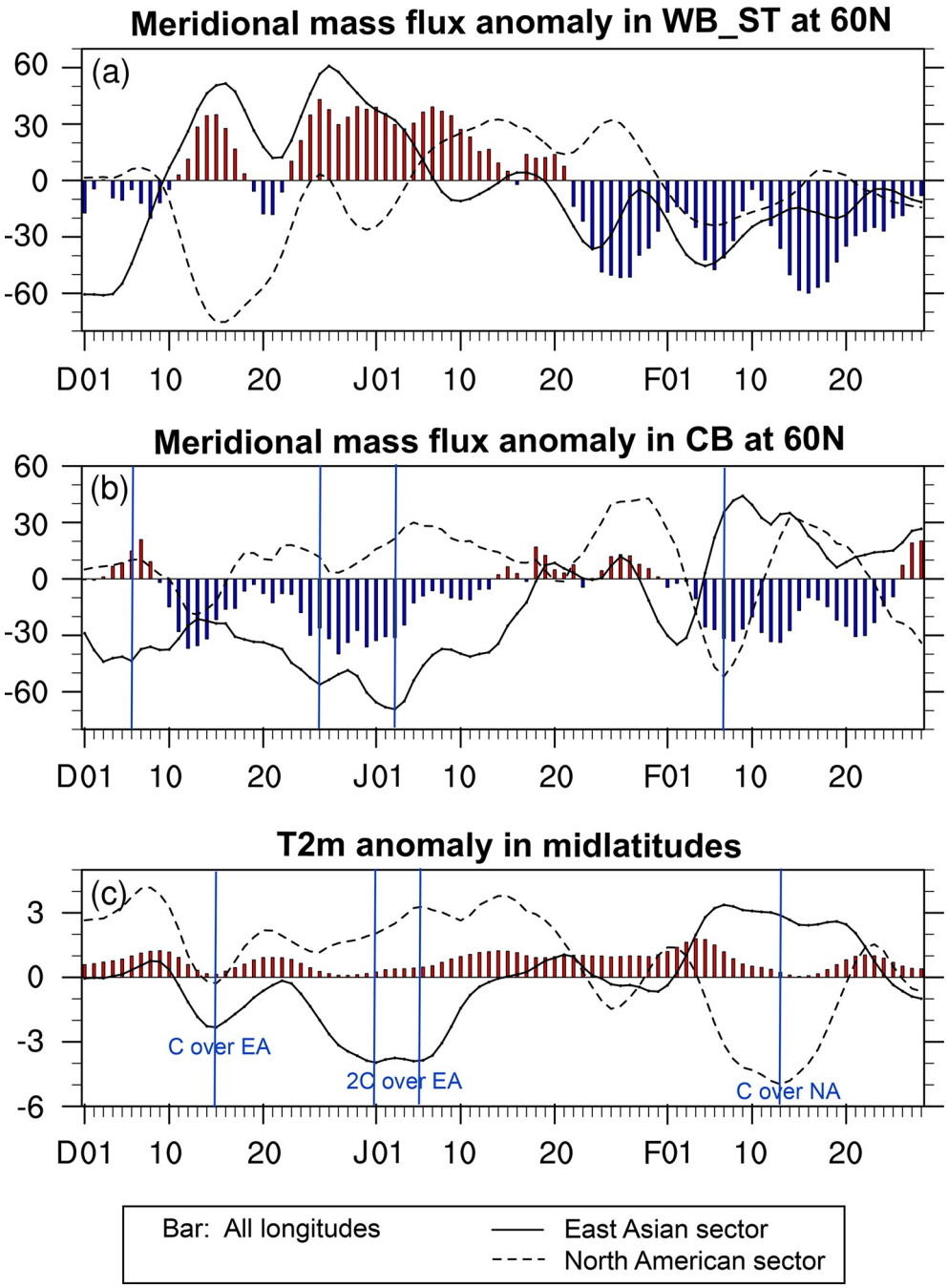

Fig. 4. Time series of zonally integrated meridional mass flux anomalies across 60°N (units: 10^9 kg s^{-1}) (a) within the WB_ST and (b) CB of the IMC, and zonal mean (c) midlatitude surface temperature anomaly (units: K) over all longitudinal bands (bars), East Asian longitudinal range (black solid curve), and North American longitudinal range (black dashed curve) from 1 December 2020 to 28 February 2021. The zonally integrated meridional mass flux anomalies within the WB_ST over all longitudes are magnified by a scale factor of 10. Vertical blue lines indicate the negative peaks in the time series of the CB and surface air temperature. "C over EA" indicates the cold event occurred in East Asia and "2C over EA" indicates the two extreme cold events occurred in East Asia; " C over NA" indicate the cold event occurred in North America. "C over EA "indicates the cold event occurred in East Asia and "2C over EA" indicates the two extreme cold events occurred in East Asia; " C over NA" indicate the cold event occurred in North America.

sure) in the middle latitudes of East Asia (Fig. 3d), which further led to the stratospheric polar vortex shift towards lower latitudes over East Asia. The reverse of the temperature gradient and zonal wind were also observed mainly over the East Asian sector (Figs. 3d and 3e) rather than the North American sector (Figs. 3h). Therefore, it is the anomalously strong

WB of the IMC in the East Asian sector that gave rise to the displacement-type SSW event on 4 January 2021.

The longitudinal profile of the monthly mean anomalies of meridional mass transport across 60°N and the Plumb wave-activity fluxes at various isentropic layers (Figs. 5a–5c) also show that in December, which is before the SSW event, wave-activity fluxes were anomalously upward and converged at levels above 350 K, mainly in the East Asian sector. Since the anomalously warm temperatures over North America were in accompaniment with the successive cold events over East Asia, resembling the surface air temperature response to strengthened wavenumber-1 wave pattens, the wavenumber-1 planetary wave should be the main contributor to the anomalous IMC and thus the occurrence of the displacement-type SSW event, as reported by Lu et al. (2021).

3.3. *The coupling between the CB and WB responsible for the impact of the SSW event on the extreme cold events*

The weaker stratospheric polar vortex during the displacement-type SSW event also played a positive role in intensifying the extreme cold events over East Asia in the beginning of January and promoting the occurrence of the extreme cold event over North America in February. The physical process involved in such a downward impact from the stratosphere on the tropospheric weather can be easily understood in view of mass changes in the upper levels and in the total column induced by the IMC variability.

Firstly, we see that the positive mass anomalies in the polar stratosphere since 23 December (Figs. 3a and 4a) correspond well to the southward expansion of the polar surface high anomalies from 25 December to 10 January (Figs. 3b and 3e). The in-phase relation between the stratospheric mass and surface pressure (proportional to total column mass) suggests that the additional polar air mass in the upper levels is able to increase the total column mass and thus the polar surface high, promoting its southward intrusion. This may partly explain why the intensity and duration of the equatorward cold air transport during 25 December–10 January significantly exceeded those in 10–20 December.

Secondly, the continuously positive mass anomalies in the polar stratosphere until mid-February (Figs.3a and Fig. 4a) were also in-phase with the positive surface pressure anomalies in the polar region and the small negative anomalies in the midlatitudes (Fig. 3b), suggesting that the additional warm air mass in the upper layers associated with the SSW event made important contributions to extending the negative phase of the AO at surface. A negative phase of the AO is well recognized as a favorable condition for the occurrence of strong cold surges in midlatitudes. Moreover, it is seen from Fig. 3h that after the westerlies reversed in the East Asian sector during the displacement-type SSW event, tropospheric planetary waves can propagate upward only through the North American sector, where the westerlies were still existent. It is seen from Fig. 5b that upward wave fluxes in January were found in the central North Pacific and zonal convergence of wave fluxes at levels above 350 K occurred mainly in the North American sector. These upward propagated waves strengthened the poleward warm air transport into the polar vortex from the North American side during the three weeks following the occurrence of the SSW event (i.e., 5 January–1 February) (Figs. 3h and 4a). Then after the upper warm air reached the high latitudes, the polar temperature at 50 hPa and total air mass above 400 K were significantly increased again around 1–10 February in the North American sector (Fig. 3g). Due to the mass gain in the upper levels, the surface pressure over the North American sector also reached a maximum and moved southward in the same period (contours in bottom panel of Fig. 3h), corresponding to the blocking high strengthening over the Baffin Bay and Greenland (Zhang et al., 2021). The anomalous high pushed more cold air equatorward, consistent with the strengthened equatorward mass transport at lower isentropic layers (Fig. 3h). In brief, the AO negative phase and the strengthening of the IMC in the North American sector, closely related to the displacement-type SSW event, collaboratively contributed to the record-breaking cold event that occurred in North America in mid-February.

Therefore, from the IMC view, the extreme cold events over East Asia and North America have close relationships with the displacement-type SSW event, both of which are results of coupling variations of the WB and CB of the IMC at different continental sectors.

4. Other possible influencing factors of the anomalous IMC

Two questions still remain: 1) what are the main tropospheric factors leading to the stronger wavenumber-1 wave-driven IMC and thus the related surface temperature patterns (i.e., cold midlatitude East Asia and warm midlatitude North America) from mid-December to early-January? 2) Besides the downward impact from the SSW, what are the roles of tropospheric factors in contributing to the IMC and its related extreme cold event over North America in February? To tentatively address the remaining questions, we conducted a composite analysis to investigate the historical features of the IMC during winters characterized by boundary forcing mechanisms including La Niña, warm SSTs over the North Pacific and the North Atlantic, low sea ice extent, and the occurrence of displacement-type SSW events, which are the main features found in the 2020/21 winter. Note that with the long-term trend removed, the unique anomalies of the Niño-3.4 index, SSTs over the North Pacific and the North Atlantic, and low sea ice extent shown in Fig. 1 can still be seen. Nevertheless, since the occurrence of extreme cold events may be related to global warming (Dai et al., 2021; Zhang et al., 2021) and many of the defining characteristics of this winter are based on the "history records" (the climatology) without removing the global

warming trend, the composite analysis in this section is based on the raw indices without detrending. The years, months, and days to be used in the composites are listed in Table 1. Figures 5d–r illustrate the longitudinal profile of the monthly mean anomalies of meridional mass transport and Plum wave-activity fluxes at 60°N at various isentropic layers composited for winters with various forcing.

It is seen from Figs. 5a and 5b that during the period from December 2020 to January 2021, the equatorward air transport was anomalously strong via the entire longitudinal span of East Asia and is responsible for the extreme cold conditions there in the early winter months. Such strengthened equatorward air transport could be mainly contributed from the low autumn Arctic sea ice extent, as indicated by the significant negative meridional mass flux anomalies across 60°N in 60°–120°E (Fig. 5m). One way of understanding the effect of Arctic sea ice on the enhanced cold air transport route is via the formation of Ural blocking during the first extreme cold event over East Asia (Lu et al., 2021; Zhang et al., 2021), since the Arctic sea ice loss in the Barents and Kara Seas can enhance the Ural blocking through generating a wave train (Luo et al., 2016; Zhang et al., 2021). In addition, the equatorward meridional mass fluxes also tend to be stronger over the Eurasian span in associa-

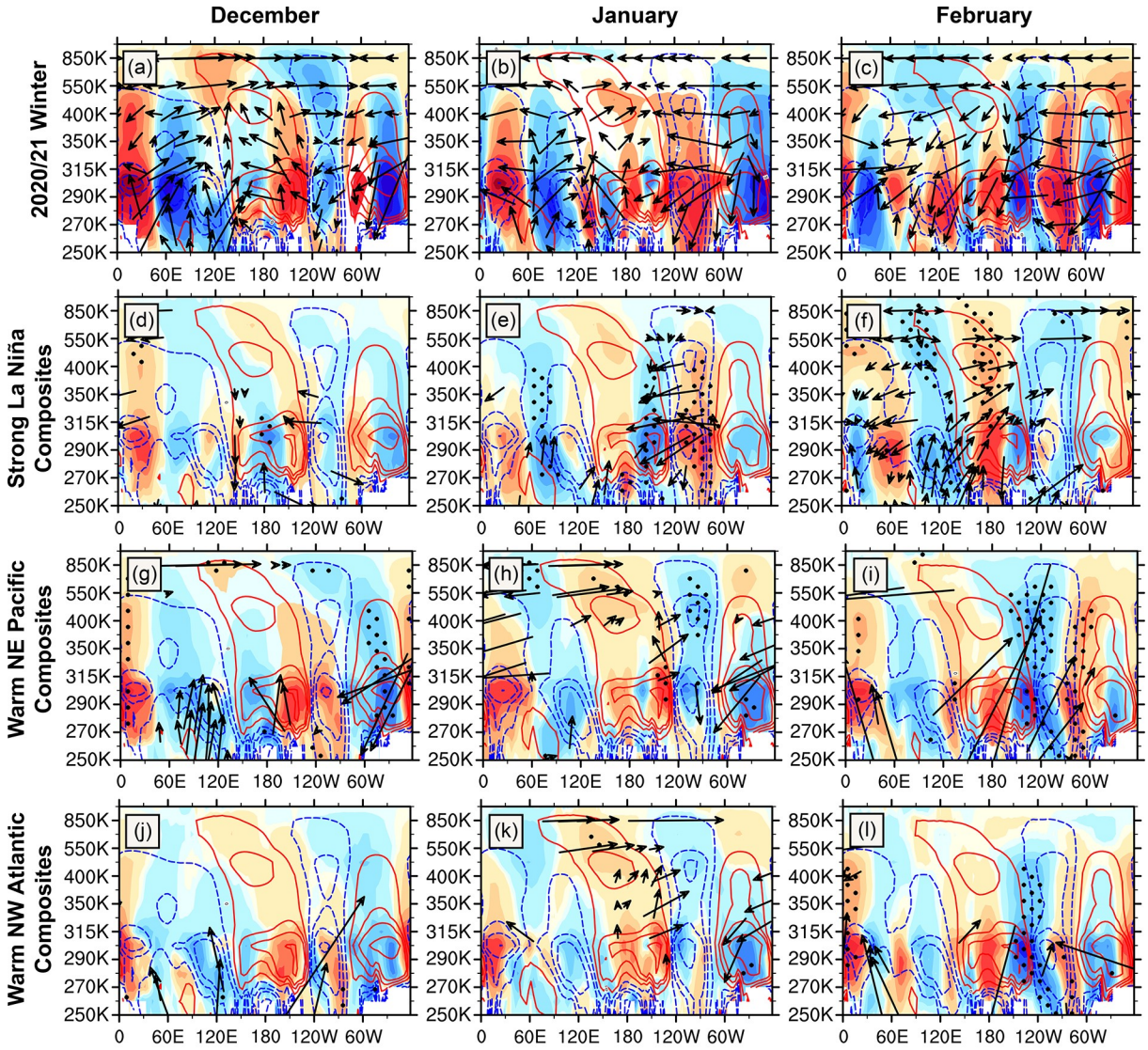

Fig. 5. The longitudinal profile of the monthly mean anomalies of meridional mass fluxes across 60°N (shadings, 10^9 kg s^{-1}, positive/negative values indicate anomalously northward/southward mass fluxes) and Plum wave-activity fluxes (vectors, m^2 s^{-2}) at various isentropic layers). (a–c) Observations in the 2020/21 winter; Composites for (d–f) moderate and strong La Niña years; (g–i) Warm northwestern Pacific (120°–160°W, 20°–60°N) SST years; (j–l) Warm northeastern Atlantic (50°–80°W, 20°–60°N) SST years; (m–o) Low autumn sea ice extent years; (p–r) Composites for the period one month before, one month after, and two months after the central dates of displacement-type SSW events. Years for composites are listed in Table 1. Dots in (d–r) indicate composites above the 90% confidence level, and only the composites of wave-activity fluxes above the 90% confidence level are shown. The Student's t-test is used for the statistical significance test. Contours are the winter climatology of meridional mass transport at 60°N (10^9 kg s^{-1}).

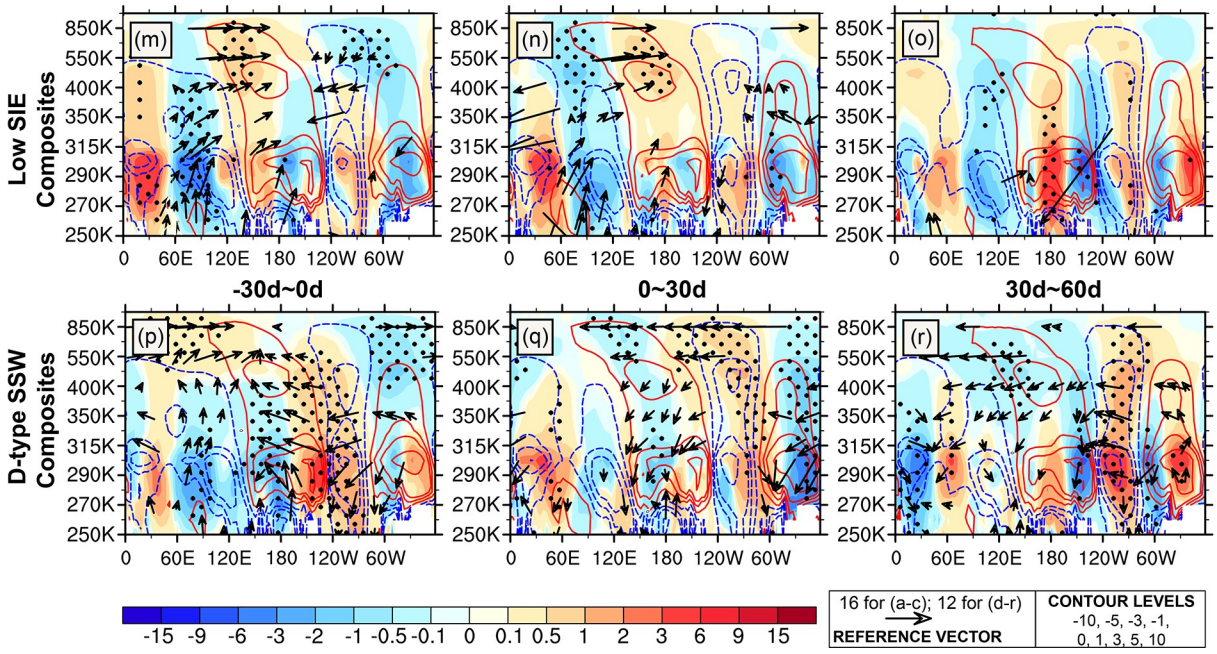

Fig. 5. (Continued).

Table 1. The winters, months, and days used for composite analysis in Fig. 5.

Winters Preceded by Low September SIE	La Niña Winters	Warm Northwestern Pacific Months			Warm Northeastern Atlantic Months			Central Dates of Displacement-type SSW
		DEC	JAN	FEB	DEC	JAN	FEB	
2007/08 2008/09	1988/89	2014	2005	2005	2014	2007	2014	1980/03/01
2010/11 2011/12	1995/96	2015	2014	2014	2015	2014	2015	1981/03/04
2012/13 2015/16	1998/99	2018	2015	2015	2016	2015	2016	1981/12/04
2016/17 2017/18	1999/2000	2019	2016	2016	2017	2016	2017	1984/02/24
2018/19 2019/20	2007/08	2020	2018	2018	2019	2017	2018	1987/01/23
2020/21	2010/11		2019	2019	2020	2020	2019	1998/12/15
	2011/12		2020	2020		2021	2020	2000/03/20
	2020/21		2021				2021	2001/12/30
								2002/02/17
								2004/01/05
								2006/01/21
								2007/02/24
								2008/02/22
								2019/01/01
								2021/01/04

tion with Decembers with above-normal SST over the northeastern Pacific and northwestern Atlantic (Figs. 5g and 5j). La Niña tends to be associated with weaker equatorward cold air transport in December and stronger equatorward cold air transport in January (Figs. 5d and 5e). However, these relationships are not statistically significant. In the meantime, the climatological route of cold air via the longitudinal span of North America (90°–150°W) was weakened in December 2021, as indicated by the positive anomalies of meridional mass fluxes below 270 K (Fig. 4a). The weakening of equatorward transport of cold air is within the lower isentropic layers, in contrast with the strengthening of equatorward transport above. A likely explanation could be the lack of cold air mass locally, potentially attributed to the warm SST over the northeastern Pacific (Fig. 5g). We can conclude that the decreased temperature gradient and blockings induced by low autumn Arctic sea ice make the most contributions to the East Asian cold events, whereas the local warming effect of abnormally warm SST over the northeastern Pacific is the main factor leading to the anomalous warmth in North America in December.

We turn now to look at the upper levels. The stronger upward propagated wave fluxes into the upper stratosphere observed in December and January in the 2020/21 winter (Figs. 5a and 5b) appear to be highly consistent with those associated with low sea ice extent, as shown Figs. 5m and 5n. It is also seen that the low SIE-related meridional mass flux anomalies in the stratospheric layers above 400 K tend

to be in-phase with the climatological field, leading to a stronger WB in the stratosphere. These results suggest that the sea ice loss in the Barents-Kara Sea during autumn and the following early winter also played an important role in promoting the upward propagation of planetary waves and thus disturbing the stratospheric polar vortex in early winter, as stated in previous studies (Sun et al., 2015; Lu et al., 2021). The warm SST over the northeastern Pacific, as a wave source, can also strengthen the upward propagation of waves in 60°–120°E, but the strengthening is confined within tropospheric levels below 315 K. The pattern of meridional mass flux anomalies as well as the features of wave activities in this early winter strongly resemble the composite pattern that occurred one month before the displacement-type SSW events (Fig. 5p) and provide favorable conditions for the occurrence of the SSW event in the beginning of January.

In February, which is after the displacement-type SSW event, the equatorward mass fluxes at 60°N became anomalously strong over the North American continent (150°–90°W) (Fig. 5c) and were responsible for the extreme cold event there. Comparison with isentropic meridional mass flux anomalies associated with various forcing mechanisms, shown in Figs. 5f, 5i, 5l, and 5o, reveals that the abnormally warm SSTs over both the northeastern Pacific and northwestern Atlantic act to enhance the equatorward cold air mass transport in the region of 120°–90°W. The warm northeastern Pacific SSTs induced an anticyclonic anomaly, thus strengthening the northerlies across the North American continent, according to Zhang et al. (2021). La Niña also tends to make positive, but not statistically significant, contributions to the stronger equatorward mass fluxes at 60°N over the North American sector, which can be explained by their indirect and complicated relationship with extratropical warm SSTs (Matsumura and Kosaka, 2019; Chen et al., 2020) and atmospheric circulation changes over the North Pacific and Atlantic (e.g., the Pacific–North American teleconnection pattern and strength and location of the jet) (Lau and Nath, 2001; Lin and Derome, 2004; Soulard et al., 2019; Mezzina et al., 2020). The downward impact from the displacement-type SSW event, as discussed in previous section, however, is responsible for the strengthening of equatorward cold air mass transport mainly along the west coast of North America (150°–120°W) (Fig. 5r). Though this cold air intrusion is slightly westward, the meridionally oriented Rocky Mountains can guide the polar cold air southward where it can merge into the westerlies, leading to temperature drops over most of the continent. Low Arctic sea ice also tends to induce negative meridional mass fluxes along the west coast of North America, but this effect is not statistically significant (Fig. 5m). Nevertheless, the role of sea ice might be amplified together with SSW events, according to Zhang et al. (2020) who stated that North American cold events tend to occur more frequently following SSW events in the presence of low Barents–Kara Sea sea ice. Therefore, for the North American extreme cold event in February of 2021, the extratropical warm ocean forcing intensifies the equatorward cold air branch over the central and eastern parts of North America. The downward impact from displacement-type SSW events intensifies the equatorward cold air branch over the North American west coast. The autumn sea ice may also play a role, along with the occurrence of SSW.

5. Concluding remarks

Three striking and impactful extreme cold wave events successively occurred across East Asia and North America in the mid-winter of 2020/21. The isentropic mass circulation (IMC), a semi-Lagrangian framework of atmospheric circulation, is utilized to understand the physical mechanism of these extreme cold events as well as the relations between the cold events and the displacement-type SSW event that occurred on 4 January 2021. Tentative analysis on the possible influence from the boundary conditions (sea surface temperatures and sea ice anomalies) to the IMC variation and cold events has also been conducted. Our main findings from this case are summarized in Fig. 6.

First of all, the cold temperatures in the midlatitudes, as well as their out-of-phase relation with surface temperature anomalies over the high latitudes, are closely linked to the day-to-day intensity variability of the equatorward cold air branch of the IMC (CB). The extremely strong equatorward cold air transport along the climatological cold air pathways over East Asia and the west coast of North America in the 2020/21 winter resulted in a significant net increase of cold air mass in the midlatitudes, leading to the extreme cold events. The vertical dynamical coupling between the CB at lower isentropic levels and the poleward warm air branch of the IMC (WB) at upper levels can explain the interaction between cold extremes and the displacement-type SSW event.

Combining the analysis results of the other influencing factors on the waves and IMC variability, we briefly describe the key physical processes involved in these consecutive extreme cold events in the 2020/21 winter in sequence as follows:

In the early winter:

i) The two cold surges over East Asia in early winter were results of intensification of the cold air transport there, which corresponds to the Arctic sea ice loss in autumn.

ii) The weakened cold air transport over North America associated with warmer northeastern Pacific sea surface temperatures (SSTs) explains the concurrent anomalously warm conditions in North America in December.

iii) The cold events over East Asia and warm temperatures over North America, together with the sea ice loss in autumn, favor the intensification of a wavenumber-1 planetary wave in the lower troposphere and its upward propagation. This drove a long-lasting stronger poleward transport of warm air into the polar stratosphere, resulting in the polar vortex break in the type of displacement towards East Asia.

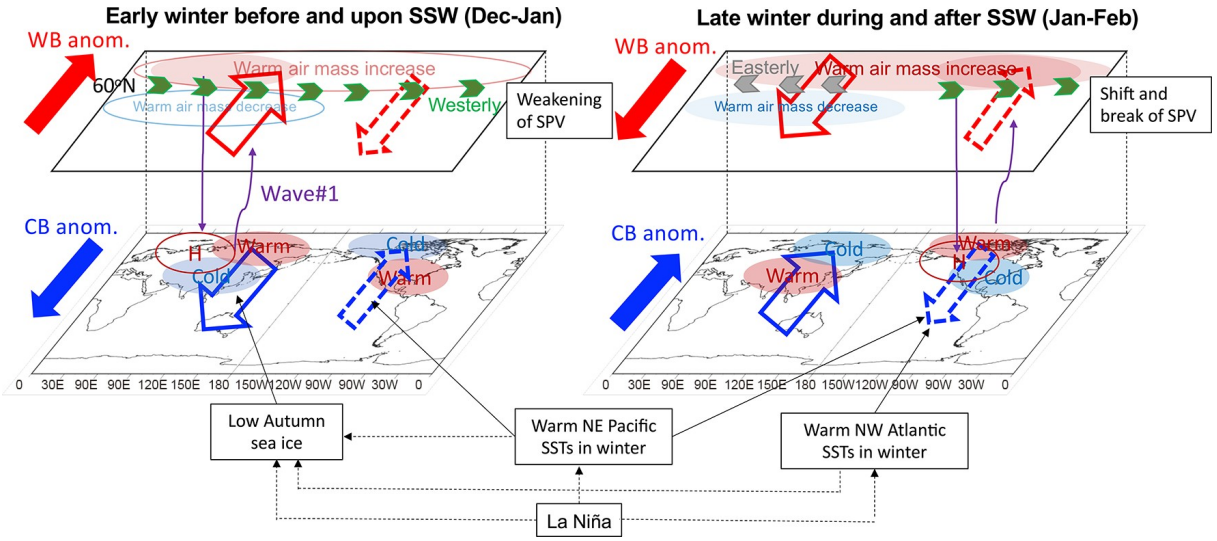

Fig. 6. Schematic figure illustrating the interactive dynamical processes between the variations of the stratospheric polar vortex and extratropical surface temperature responsible for the occurrence of the three extreme cold events from the IMC perspective, and the possible factors influencing the anomalous variations of the IMC in winter.

The extreme cold event over East Asia in the beginning of January was also intensified and prolonged by the additional air mass gain in the stratosphere associated with the strengthened WB upon the displacement-type SSW event.

In February:

i) The cold event over North America in February after the displacement-type SSW event turns out to be influenced by the local modulation of the IMC by the wave-mean flow interaction during the displacement-type SSW event as well as the negative phase of the AO induced by the SSW event providing favorable conditions.

ii) In addition to the downward impact from the stratosphere, the forcing from the extratropical warm SSTs mainly over the northeastern Pacific and northwestern Atlantic also makes contributions to strengthening the equatorward cold air transport over the North American route.

It is noteworthy that our results do not show robust relationships between La Niña itself and the IMC and the subsequent three extreme cold events in the 2020/21 winter. Such inconsistent impacts of ENSO on winter weather and climate has recently drawn scientists' attention (Ma and Chen, 2021). One reason for the inconsistent climate impacts of ENSO could be that the analyses in this study only focus on the independent impact of various forcing mechanisms on the IMC. But in fact, these forcing mechanisms can have active interactions. For instance, Arctic sea ice variation is associated with ENSO (Jevrejeva et al., 2003; Liu et al., 2004; Hu et al., 2016; Chen et al., 2020). Cold eastern equatorial Pacific SSTs in the previous summer can lead to persistent tropical Atlantic cooling (Matsumura and Kosaka, 2019) and intensification of the upper-level high in the polar region (Ding et al., 2017; Baxter et al., 2019; Huang et al., 2021; Luo et al., 2021), which result in Arctic sea ice loss in autumn. This looks to be the case for 2020 when the Niño-3.4 index is below normal in summer while the sea ice extent is extremely low in autumn. ENSO forcing during mid-winter can also affect the extratropical SST anomalies, particularly in late winter or early spring, via modulating atmospheric circulation changes over the North Pacific and Atlantic and thus the heat exchange across the local sea–air interface (Lau and Nath, 2001). In addition, the below-normal autumn Arctic sea ice in 2020, particularly over the Barents Sea, has been reported to be related to the warm North Atlantic and North Pacific SST anomalies via enhanced poleward intrusion of the warm water into these two ocean regions (Zhang et al., 2021). Moreover, these forcing mechanisms always cooperatively, rather than independently, change the winter climate. For instance, the ENSO-induced Rossby wave train can cooperate with the Arctic sea ice to influence the Eurasian winter temperature (Matsumura and Kosaka, 2019). The relationship between the East Asian winter monsoon and La Niña can be tightened by the cold phase of the Pacific Decadal Oscillation (Wang et al., 2008; Kim et al., 2014), which is also the case for the 2020/21 winter. The combined effects of the tropical and extratropical ocean forcing mechanisms, sea ice, and the stratospheric polar vortex on the IMC and continental extreme cold events need further investigation through future studies.

As the global warming process will continue unequivocally, the land–sea thermal contrast will increase, sea ice will melt with large regional differences, etc. These effects will continue to strengthen planetary wave activities, which are the main driving force of the IMC. One may expect changes in the intensity and intraseasonal variations of the IMC over an entire latitude band or specific regions, which might indicate more occurrences of extreme cold events. This is also an interesting question that should be investigated in the future as longer data records become available.

Acknowledgements. The meteorological variable fields from ERA5 datasets, Niño-3.4 index data, sea ice extents, and SST

data used in this work are available from the official websites of the ECMWF (https://cds.climate.copernicus.eu/cdsapp#!/home), NSIDC (http://nsidc.org/data/seaice/data_summaries.html), and NOAA (https://psl.noaa.gov/data/timeseries/monthly/NINO34/; https://psl.noaa.gov/data/gridded/data.noaa.oisst.v2.highres.html). This work was supported by grants from the National Key R&D Program of China (Grant No. 2019YFC1510201), National Natural Science Foundation of China (Grant Nos. 42075052 and 42088101), and the Natural Science Foundation of Jiangsu Province (Grants No. BK20211288).

REFERENCES

Abdillah, M. R., Y. Kannao, and T. Iwasaki, 2017: Tropical–extratropical interactions associated with east Asian cold air outbreaks. Part I: Interannual variability. *J. Climate*, **30**, 2989–3007, https://doi.org/10.1175/JCLI-D-16-0152.1.

Baxter, I., and Coauthors, 2019: How tropical pacific surface cooling contributed to accelerated sea ice melt from 2007 to 2012 as ice is thinned by anthropogenic forcing. *J. Climate*, **32**, 8583–8602, https://doi.org/10.1175/JCLI-D-18-0783.1.

Cai, M., Y. Y. Yu, Y. Deng, H. M. van den Dool, R. Ren, S. Saha, X. R. Wu, and J. Huang, 2016: Feeling the pulse of the stratosphere: An emerging opportunity for predicting continental-scale cold-air outbreaks 1 month in advance. *Bull. Amer. Meteor. Soc.*, **97**, 1475–1489, https://doi.org/10.1175/BAMS-D-14-00287.1.

Charlton, A. J., and L. M. Polvani, 2007: A new look at stratospheric sudden warmings. *Part I: Climatology and modeling benchmarks. J. Climate*, **20**, 449–469, https://doi.org/10.1175/JCLI3996.1.

Chen, S. F., R. G. Wu, W. Chen, and B. Yu, 2020: Influence of winter Arctic sea ice concentration change on the El Niño–Southern Oscillation in the following winter. *Climate Dyn.*, **54**(1–2), 741–757, https://doi.org/10.1007/s00382-019-05027-1.

Choi, H., B.-M. Kim, and W. Choi, 2019: Type classification of sudden stratospheric warming based on pre- and postwarming periods. *J. Climate*, **32**, 2349–2367, https://doi.org/10.1175/jcli-d-18-0223.1.

Choi, H., J.-H. Kim, B.-M. Kim, and S.-J. Kim, 2021: Observational evidence of distinguishable weather patterns for three types of sudden stratospheric warming during northern winter. *Frontiers in Earth Science*, **9**, 625868, https://doi.org/10.3389/feart.2021.625868.

Dai, G. K., C. X. Li, Z. Han, D. H. Luo, and Y. Yao, 2021: The nature and predictability of the East Asian extreme cold events of 2020/21. *Adv. Atmos. Sci.*, in press, https://doi.org/10.1007/s00376-021-1057-3.

Ding, Q. H., and Coauthors, 2017: Influence of high-latitude atmospheric circulation changes on summertime Arctic sea ice. *Nature Climate Change*, **7**, 289–295, https://doi.org/10.1038/nclimate3241.

Francis, J. A., and S. J. Vavrus, 2012: Evidence linking Arctic amplification to extreme weather in mid-latitudes. *Geophys. Res. Lett.*, **39**(6), L06801, https://doi.org/10.1029/2012gl051000.

Gallimore, R. G., and D. R. Johnson, 1981: A numerical diagnostic model of the zonally averaged circulation in isentropic coordinates. *J. Atmos. Sci.*, **38**, 1870–1890, https://doi.org/10.1175/1520-0469(1981)038<1870:ANDMOT>2.0.CO;2.

He, S. P., and H. J. Wang, 2013: Oscillating relationship between the East Asian winter monsoon and ENSO. *J. Climate*, **26**(24), 9819–9838, https://doi.org/10.1175/jcli-d-13-00174.1.

Hersbach, H., and Coauthors, 2020: The ERA5 global reanalysis. *Quart. J. Roy. Meteor. Soc.*, **146**, 1999–2049, https://doi.org/10.1002/qj.3803.

Hoerling, M. P., and A. Kumar, 1997: Why do North American climate anomalies differ from one El Niño event to another. . *Geophys. Res. Lett.*, **24**, 1059–1062, https://doi.org/10.1029/97GL00918.

Hu, C. D., S. Yang, Q. G. Wu, Z. N. Li, J. W. Chen, K. Q. Deng, T. T. Zhang, and C. Y. Zhang, 2016: Shifting El Niño inhibits summer Arctic warming and Arctic sea-ice melting over the Canada Basin. *Nature Communications*, **7**, 11721, https://doi.org/10.1038/ncomms11721.

Huang, J. L., and W. S. Tian, 2019: Eurasian cold air outbreaks under different arctic stratospheric polar vortex strengths. *J. Atmos. Sci.*, **76**(5), 1245–1264, https://doi.org/10.1175/JAS-D-18-0285.1.

Huang, J. L., P. Hitchcock, A. C. Maycock, C. M. McKenna, and W. S. Tian, 2021: Northern hemisphere cold air outbreaks are more likely to be severe during weak polar vortex conditions. *Communications Earth & Environment*, **2**, 147, https://doi.org/10.1038/s43247-021-00215-6.

Iwasaki, T., and Y. Mochizuki, 2012: Mass-weighted isentropic zonal mean equatorward flow in the northern hemispheric winter. *SOLA*, **8**, 115–118, https://doi.org/10.2151/sola.2012-029.

Iwasaki, T., T. Shoji, Y. Kanno, M. Sawada, M. Ujiie, and K. Takaya, 2014: Isentropic analysis of polar cold airmass streams in the northern hemispheric winter. *J. Atmos. Sci.*, **71**, 2230–2243, https://doi.org/10.1175/JAS-D-13-058.1.

Jevrejeva, S., J. C. Moore, and A. Grinsted, 2003: Influence of the Arctic Oscillation and El Niño-Southern Oscillation (ENSO) on ice conditions in the Baltic Sea: The wavelet approach. *J. Geophys. Res.*, **108**(D21), 4677, https://doi.org/10.1029/2003jd003417.

Joh, Y., and E. Di Lorenzo, 2017: Increasing coupling between NPGO and PDO leads to prolonged marine heatwaves in the Northeast Pacific. *Geophys. Res. Lett.*, **44**, 11663–11671, https://doi.org/10.1002/2017GL075930.

Johnson, D. R., 1989: The forcing and maintenance of global monsoonal circulations: An isentropic analysis. *Advances in Geophysics*, **31**, 43–316, https://doi.org/10.1016/S0065-2687(08)60053-9.

Kenyon, J., and G. C. Hegerl, 2008: Influence of modes of climate variability on global temperature extremes. *J. Climate*, **21**, 3872–3889, https://doi.org/10.1175/2008JCLI2125.1.

Kidston, J., A. A. Scaife, S. C. Hardiman, D. M. Mitchell, N. Butchart, M. P. Baldwin, and L. J. Gray, 2015: Stratospheric influence on tropospheric jet streams, storm tracks and surface weather. *Nature Geoscience*, **8**, 433–440, https://doi.org/10.1038/ngeo2424.

Kim, J.-W., S.-W. Yeh, and E.-C. Chang, 2014: Combined effect of El Niño-Southern Oscillation and Pacific Decadal Oscillation on the East Asian winter monsoon. *Climate Dyn.*, **42**(3), 957–971, https://doi.org/10.1007/s00382-013-1730-z.

Lau, N.-C., and M. J. Nath, 2001: Impact of ENSO on SST variability in the North Pacific and North Atlantic: Seasonal dependence and role of extratropical sea–air coupling. *J. Climate*, **14**(13), 2846–2866, https://doi.org/10.1175/1520-0442

(2001)014<2846:IOEOSV>2.0.CO;2.

Lee, S. H., 2021: The January 2021 sudden stratospheric warming. *Weather*, **76**, 135–136, https://doi.org/10.1002/wea.3966.

Lehtonen, I., and A. Y. Karpechko, 2016: Observed and modeled tropospheric cold anomalies associated with sudden stratospheric warmings. *J. Geophys. Res.*, **121**, 1591–1610, https://doi.org/10.1002/2015JD023860.

Lin, H., and J. Derome, 2004: Nonlinearity of the extratropical response to tropical forcing. *J. Climate*, **17**, 2597–2608, https://doi.org/10.1175/1520-0442(2004)017<2597:NOTERT>2.0.CO;2.

Liu, J. P., J. A. Curry, and Y. Y. Hu, 2004: Recent arctic sea ice variability: Connections to the arctic oscillation and the ENSO. *Geophys. Res. Lett.*, **31**(9), L09211, https://doi.org/10.1029/2004gl019858.

Liu, J. P., J. A. Curry, H. J. Wang, M. R. Song, and R. M. Horton, 2012: Impact of declining Arctic sea ice on winter snowfall. *Proceedings of the National Academy of Sciences of the United States of America*, **109**(11), 4074–4079, https://doi.org/10.1073/pnas.1114910109.

Lu, Q., J. Rao, Z. Q. Liang, D. Guo, J. J. Luo, S. M. Liu, C. Wang, and T. Wang, 2021: The sudden stratospheric warming in January 2021. *Environmental Research Letters*, **16**, 084029, https://doi.org/10.1088/1748-9326/ac12f4.

Luo, B. H., D. H. Luo, A. G. Dai, I. Simmonds, and L. X. Wu, 2021: A connection of winter Eurasian cold anomaly to the modulation of Ural blocking by ENSO. *Geophys. Res. Lett.*, **48**, e2021GL094304, https://doi.org/10.1029/2021GL094304.

Luo, D. H., Y. Q. Xiao, Y. Yao, A. G. Dai, I. Simmonds, and C. L. E. Franzke, 2016: Impact of Ural blocking on winter warm Arctic-cold Eurasian anomalies. Part I: Blocking-induced amplification. *J. Climate*, **29**(11), 3925–3947, https://doi.org/10.1175/jcli-d-15-0611.1.

Ma, T. J., and W. Chen, 2021: Climate variability of the East Asian winter monsoon and associated extratropical–tropical interaction: A review. *Annals of the New York Academy of Sciences*, in press, https://doi.org/10.1111/nyas.14620.

Matsumura, S., and Y. Kosaka, 2019: Arctic-Eurasian climate linkage induced by tropical ocean variability. *Nature Communications*, **10**(1), 3441, https://doi.org/10.1038/s41467-019-11359-7.

Mezzina, B., J. García-Serrano, I. Bladé, F. M. Palmeiro, L. Batté, C. Ardilouze, M. Benassi, and S. Gualdi, 2020: Multimodel assessment of the late-winter extra-tropical response to El Niño and La Niña. *Climate Dyn.*, in press, https://doi.org/10.1007/s00382-020-05415-y.

Mitchell, D. M., L. J. Gray, J. Anstey, M. P. Baldwin, and A. J. Charlton-Perez, 2013: The influence of stratospheric vortex displacements and splits on surface climate. *J. Climate*, **26**, 2668–2682, https://doi.org/10.1175/JCLI-D-12-00030.1.

NASA, 2020: 2020 Arctic Sea Ice Minimum at Second Lowest on Record. Available from https://www.nasa.gov/feature/goddard/2020/2020-arctic-sea-ice-minimum-at-second-lowest-on-record/.

Petoukhov, V., and V. A. Semenov, 2010: A link between reduced Barents-Kara sea ice and cold winter extremes over northern continents. *J. Geophys. Res.*, **115**(D21), D21111, https://doi.org/10.1029/2009jd013568.

Plumb, R. A., 1985: On the three-dimensional propagation of stationary waves. *J. Atmos. Sci.*, **42**, 217–229, https://doi.org/10.1175/1520-0469(1985)042<0217:OTTDPO>2.0.CO;2.

Rao, J., R. C. Ren, H. S. Chen, Y. Y. Yu, and Y. Zhou, 2018: The stratospheric sudden warming event in February 2018 and its prediction by a climate system model. *J. Geophys. Res.*, **123**, 13 332–13 345, https://doi.org/10.1029/2018JD028908.

Rao, J., C. I. Garfinkel, H. S. Chen, and I. P. White, 2019: The 2019 New Year stratospheric sudden warming and its real‐time predictions in multiple S2S models. *J. Geophys. Res.*, **124**, 11 155–11 174, https://doi.org/10.1029/2019JD030826.

Ropelewski, C. F., and M. S. Halpert, 1986: North American precipitation and temperature patterns associated with the El Niño/Southern Oscillation (ENSO). *Mon. Wea. Rev.*, **114**, 2352–2362, https://doi.org/10.1175/1520-0493(1986)114<2352:NAPATP>2.0.CO;2.

Sakai, K., and R. Kawamura, 2009: Remote response of the East Asian winter monsoon to tropical forcing related to El Niño–Southern Oscillation. *J. Geophys. Res.*, **114**(D6), D06105, https://doi.org/10.1029/2008jd010824.

Screen, J. A., and I. Simmonds, 2013: Exploring links between Arctic amplification and mid-latitude weather. *Geophys. Res. Lett.*, **40**(5), 959–964, https://doi.org/10.1002/grl.50174.

Shabbar, A., and M. Khandekar, 1996: The impact of el Niño‐Southern oscillation on the temperature field over Canada: Research note. *Atmos.-Ocean*, **34**, 401–416, https://doi.org/10.1080/07055900.1996.9649570.

Shabbar, A., B. Bonsal, and M. Khandekar, 1997: Canadian precipitation patterns associated with the Southern Oscillation. *J. Climate*, **10**, 3016–3027, https://doi.org/10.1175/1520-0442(1997)010<3016:CPPAWT>2.0.CO;2.

Shabbar, A., and B. Yu, 2009: The 1998 – 2000 La Niña in the context of historically strong La Niña events. *J. Geophys. Res.*, **114**, D13105, https://doi.org/10.1029/2008JD011185.

Shoji, T., Y. Kanno, T. Iwasaki, and K. Takaya, 2014: An isentropic analysis of the temporal evolution of East Asian cold air outbreaks. *J. Climate*, **27**(24), 9337–9348, https://doi.org/10.1175/JCLI-D-14-00307.1.

Sorokina, S. A., C. Li, J. J. Wettstein, and N. G. Kvamstø, 2016: Observed atmospheric coupling between Barents Sea ice and the warm-Arctic cold-Siberian anomaly pattern. *J. Climate*, **29**(2), 495–511, https://doi.org/10.1175/jcli-d-15-0046.1.

Soulard, N., H. Lin, and B. Yu, 2019: The changing relationship between ENSO and its extratropical response patterns. *Scientific Reports*, **9**, 6507, https://doi.org/10.1038/s41598-019-42922-3.

Sun, C. H., S. Yang, W. J. Li, R. N. Zhang, and R. G. Wu, 2016: Interannual variations of the dominant modes of East Asian winter monsoon and possible links to Arctic sea ice. *Climate Dyn.*, **47**(1–2), 481–496, https://doi.org/10.1007/s00382-015-2851-3.

Sun, L. T., C. Deser, and R. A. Tomas, 2015: Mechanisms of stratospheric and tropospheric circulation response to projected Arctic sea ice loss. *J. Climate*, **28**, 7824–7845, https://doi.org/10.1175/JCLI-D-15-0169.1.

Thompson, D. W. J., M. P. Baldwin, and J. M. Wallace, 2002: Stratospheric connection to northern Hemisphere wintertime weather: Implications for prediction. *J. Climate*, **15**, 1421–1428, https://doi.org/10.1175/1520-0442(2002)015<1421:SCTNHW>2.0.CO;2.

Tomassini, L., E. P. Gerber, M. P. Baldwin, F. Bunzel, and M. Giorgetta, 2012: The role of stratosphere-troposphere coupling in the occurrence of extreme winter cold spells over

northern Europe. *Journal of Advances in Modeling Earth Systems*, **4**, M00A03, https://doi.org/10.1029/2012MS000177.

Townsend, R. D., and D. R. Johnson, 1985: A diagnostic study of the isentropic zonally averaged mass circulation during the first GARP global experiment. *J. Atmos. Sci.*, **42**, 1565–1579, https://doi.org/10.1175/1520-0469(1985)042<1565:ADSOTI>2.0.CO;2.

Wang, B., R. G. Wu, and X. H. Fu, 2000: Pacific-East Asian teleconnection: How does ENSO affect East Asian climate. . *J. Climate*, **13**(9), 1517–1536, https://doi.org/10.1175/1520-0442(2000)013<1517:peathd>2.0.co;2.

Wang, L., W. Chen, and R. H. Huang, 2008: Interdecadal modulation of PDO on the impact of ENSO on the East Asian winter monsoon. *Geophys. Res. Lett.*, **35**(20), L20702, https://doi.org/10.1029/2008gl035287.

Yao, Y., D. H. Luo, A. G. Dai, and I. Simmonds, 2017: Increased quasi stationarity and persistence of winter Ural blocking and Eurasian extreme cold events in response to Arctic warming. Part I: Insights from observational analyses. *J. Climate*, **30**(10), 3549–3568, https://doi.org/10.1175/jcli-d-16-0261.1.

Yu, Y. Y., and R. C. Ren, 2019: Understanding the variation of stratosphere–troposphere coupling during stratospheric northern annular mode events from a mass circulation perspective. *Climate Dyn.*, **53**(9-10), 5141–5164, https://doi.org/10.1007/s00382-019-04675-7.

Yu, Y. Y., M. Cai, R. C. Ren, and H. M. van den Dool, 2015a: Relationship between warm airmass transport into the upper polar atmosphere and cold air outbreaks in winter. *J. Atmos. Sci.*, **72**, 349–368, https://doi.org/10.1175/JAS-D-14-0111.1.

Yu, Y. Y., R. C. Ren, and M. Cai, 2015b: Dynamic linkage between cold air outbreaks and intensity variations of the meridional mass circulation. *J. Atmos. Sci.*, **72**, 3214–3232, https://doi.org/10.1175/JAS-D-14-0390.1.

Yu, Y. Y., R. C. Ren, and M. Cai, 2015c: Comparison of the mass circulation and AO indices as indicators of cold air outbreaks in northern winter. *Geophys. Res. Lett.*, **42**, 2442–2448, https://doi.org/10.1002/2015GL063676.

Yu, Y. Y., M. Cai, C. H. Shi, and R. C. Ren, 2018a: On the linkage among strong stratospheric mass circulation, stratospheric sudden warming, and cold weather events. *Mon. Wea. Rev.*, **146**, 2717–2739, https://doi.org/10.1175/MWR-D-18-0110.1.

Yu, Y. Y., M. Cai, and R. C. Ren, 2018b: A stochastic model with a low-frequency amplification feedback for the stratospheric northern annular mode. *Climate Dyn.*, **50**, 3757–3773, https://doi.org/10.1007/s00382-017-3843-2.

Yu, Y. Y., M. Cai, R. C. Ren, and J. Rao, 2018c: A closer look at the relationships between meridional mass circulation pulses in the stratosphere and cold air outbreak patterns in northern hemispheric winter. *Climate Dyn.*, **51**, 3125–3143, https://doi.org/10.1007/s00382-018-4069-7.

Zhang, P. F., Y. T. Wu, G. Chen, and Y. Y. Yu, 2020: North American cold events following sudden stratospheric warming in the presence of low Barents–Kara Sea sea ice. *Environmental Research Letters*, **15**, 124017, https://doi.org/10.1088/1748-9326/abc215.

Zhang, X. D., Y. F. Fu, J. E. Overland, A. Rinke, T. Han, T. Vihma, and M. Y. Wang, 2021: Extreme cold events from East Asia to North America in winter 2020/21: Comparisons, causes, and future implications. *Adv. Atmos. Sci.*, in press, https://doi.org/10.1007/s00376-021-1229-1.